# Measurements of 540–1740 MHz Brightness Temperatures of Sea Ice During the Winter of the MOSAiC Campaign

Oguz Demir<sup>®</sup>, Joel T. Johnson<sup>®</sup>, *Fellow, IEEE*, Kenneth C. Jezek<sup>®</sup>, Mark J. Andrews<sup>®</sup>, *Member, IEEE*, Kenneth Ayotte, Gunnar Spreen<sup>®</sup>, *Member, IEEE*, Stefan Hendricks<sup>®</sup>, Lars Kaleschke<sup>®</sup>, Marc Oggier, Mats A. Granskog<sup>®</sup>, Allison Fong, Mario Hoppmann, Ilkka Matero, Daniel Scholz

Abstract-A ground-based ultra-wideband radiometer operating at 540, 900, 1380, and 1740 MHz was used to measure microwave thermal emissions from an Arctic sea ice floe as part of the Multidisciplinary drifting Observatory for the Study of Arctic Climate (MOSAiC) Expedition. The instrument was deployed on a drifting ice floe near 86°N, 120°E in leg 1 of the expedition (December 2019) and observed second-year ice (potentially with refrozen melt ponds) that experienced new ice growth at its base over a ten-day period. Measured circularly polarized brightness temperatures were compared with the predictions of a radiative transfer (RT) model for a layered medium consisting of ocean, growing new ice, desalinated remnant second-year ice/refrozen melt pond, and snow layers. Characteristics of the sea ice composition used in the model were determined from in-situ measurements. Comparisons of the measured and modeled wideband brightness temperatures showed good agreement consistently over the observation period and for various off-nadir observation angles. The results

Manuscript received April 23, 2021; revised July 5, 2021; accepted August 2, 2021. This work was supported in part by the National Science Foundation Office of Polar Programs under Grant OPP-1838401. The work of Gunnar Spreen was supported by the Deutsche Forschungsgemeinschaft (DFG) through the MOSAiCmicrowaveRS Project under Grant 420499875. The work of Ilkka Matero was supported by the Diatom-ARCTIC Project jointly funded by the UK Research and Innovation (UKRI) Natural Environment Research Council (NERC) and the German Federal Ministry of Education and Research (BMBF) under Grant 03F0810A. The work of Marc Oggier was supported by the NSF Award under Grant OPP-17358621735862 and the Norwegian Polar Institute. The work of Mats A. Granskog was supported by the Research Council of Norway Projects Ridges - Safe HAVens for ice-associated Flora and Fauna in a Seasonally ice-covered Arctic OCean (HAVOC) and Coordinated Arctic Acoustic Thermometry Experiment (CAATEX) under Grant 280292 and Grant 280531. (Corresponding author: Oguz Demir.)

Oguz Demir, Joel T. Johnson, Mark J. Andrews, and Kenneth Ayotte are with the ElectroScience Laboratory, The Ohio State University, Columbus, OH 43210 USA (e-mail: demir.15@osu.edu; johnson.1374@osu.edu; andrews.250@osu.edu; ayotte.4@osu.edu).

Kenneth C. Jezek is with the Byrd Polar Research Center, The Ohio State University, Columbus, OH 43210 USA (e-mail: jezek.1@osu.edu).

Gunnar Spreen is with the Institute of Environmental Physics, University of Bremen, 28359 Bremen, Germany (e-mail: gunnar.spreen@uni-bremen.de).

Stefan Hendricks, Lars Kaleschke, Allison Fong, Mario Hoppmann, Ilkka Matero, and Daniel Scholz are with the Helmholtz Center for Polar and Marine Research, Alfred Wegener Institute, 27570 Bremerhaven, Germany (e-mail: stefan.hendrick@awi.de; lars.kaleschke@awi.de; allison.fong@awi.de; mario.hoppmann@awi.de; ilkka.matero@awi.de; daniel.scholz@awi.de).

Marc Oggier is with the International Arctic Research Center, University of Alaska, Fairbanks, AK 99775 USA, and also with the Norwegian Polar Institute, Fram Centre, 9296 Tromsø, Norway (e-mail: moggier@alaska.edu). Mats A. Granskog is with the Norwegian Polar Institute, Fram Centre, 9296 Tromsø, Norway (e-mail: mats@npolar.no).

Digital Object Identifier 10.1109/TGRS.2021.3105360

demonstrate the capabilities of 0.5–2 GHz microwave radiometry for observing sea ice properties and also show the impact of a saline ice layer at the ice bottom on the measured brightness temperature.

Index Terms—Microwave radiometry, Multidisciplinary drifting Observatory for the Study of Arctic Climate (MOSAiC) expedition, remote sensing (RS), sea ice.

#### I. Introduction

SEA ice is a significant component of the cryosphere of the earth. It has numerous crucial impacts on both the climate and the global water circulation [1]. Sea ice thickness regulates the heat flow between ocean and atmosphere, and the brine rejection during sea ice growth impacts ocean salinity and can influence oceanic deep convection. Arctic sea ice extent, thickness, and volume have substantially reduced during the recent decade [2], [3]. Therefore, understanding and estimating sea ice properties is important for improving understanding and prediction of cryospheric and oceanic processes [4].

Passive microwave radiometers have been routinely used to measure ice concentration and extent using frequencies from 6 to 89 GHz [5]-[10]. Synthetic aperture radar (SAR) has also been important to interpret ice movement [11] and ice type [12], [13]. Sea ice thickness has been inferred from the combined use of infrared and optical satellite data with thermodynamic models [14]-[16]. Lidar and radar altimeter instruments from satellite-borne missions such as SAR, ICESat/ ICESat-2, and CryoSat-2 have also been used to estimate ice thickness across the full thickness range, but suffer from significant uncertainties at thicknesses less than 1 m [17]–[20]. The 1.4-GHz passive microwave radiometers of the SMOS and SMAP satellites have been used to infer ice thickness up to 1.5 m for multiyear ice and up to 0.5 m for first year ice as well as to predict snow depth [21]-[26]. Combining data from different sea ice thickness retrieval concepts have therefore been a significant approach to overcome the specific limitations of individual methods, for example, the merging of CryoSat-2 altimeter and SMOS passive microwave radiometer observations using optimal interpolation [27].

A limited number of past studies have investigated the performance of sea ice radiometry at frequencies even lower than 1.4 GHz through airborne or ship-based

1558-0644 © 2021 IEEE. Personal use is permitted, but republication/redistribution requires IEEE permission. See https://www.ieee.org/publications/rights/index.html for more information.

measurements [28], [29]. However, the use of these frequencies has not been considered for satellite remote sensing (RS) due to the excessive human-made radio frequency interference (RFI) outside the protected band that exists from 1400 to 1427 MHz. To address these challenges, the ultra-wideband microwave radiometer (UWBRAD) was developed to perform multichannel brightness temperature (TB) measurements from 0.5 to 2 GHz [30], [31]. The instrument's unique advantage is the sensing of lower band microwave signals in the presence of RFI through the use of advanced RFI detection and filtering algorithms. The 12-channel UWBRAD radiometer was deployed in airborne missions to perform observations over Greenland in 2017 [32], [33] and over Antarctica in 2018 [34]. While retrievals of sea ice thickness using these observations have been reported, the lack of simultaneous in-situ information has limited a complete demonstration of the sensing performance achieved.

In order to further explore the capabilities of 0.5–2 GHz radiometry for sea ice RS and to improve wideband emission models for an evolving sea ice floe, a ground-based four-channel version of UWBRAD (540, 900, 1380, and 1740 MHz) was built and operated on an Arctic sea ice floe as a part of the Multidisciplinary drifting Observatory for the Study of Arctic Climate MOSAiC expedition that began in October 2019 [35]. The radiometer was operated from a stationary mast with an oblique antenna orientation and was programmed to frequently observe the sky for data calibration. For ten days, UWBRAD measured a sea ice area that survived the summer melt and that likely included refrozen melt ponds. Measurements obtained during this time period are described and interpreted in this article.

Section II provides an overview of the campaign and the dataset acquired. Section III describes the sea ice emission model used for comparison with the measurements, and *in-situ* data from the measurement site is further summarized in Section IV. In Section V, model simulations and comparisons with the measurements are discussed. Finally, Section VI provides concluding comments.

# II. UWBRAD MEASUREMENTS

## A. MOSAiC Expedition

The MOSAiC expedition was conducted to better understand the processes relevant to the ocean-ice-atmosphere system in the Arctic. The year-long campaign consisted of five cruise legs, the first of which began on October 4, 2019, when the research vessel RV Polarstern [36] moored to an ice floe measuring roughly  $2.8 \times 3.8 \text{ km}^2$  in the north of the Laptev Sea (Fig. 1). The ice floe was estimated to have formed in the north of the New Siberian Islands at the beginning of December 2018 and survived the summer melt before its drift toward the central Arctic [37]. During Leg 1 of the campaign (from October to December), the ice floe drifted from 84.6°N, 136.2°E to 86.7°N and 113.4°E. The Central Observatory research camp installed on the floe served as the main base for research activities and comprised numerous measurement stations such as the RS site. Several groundbased microwave RS instruments including UWBRAD were deployed and operated at this site [38].

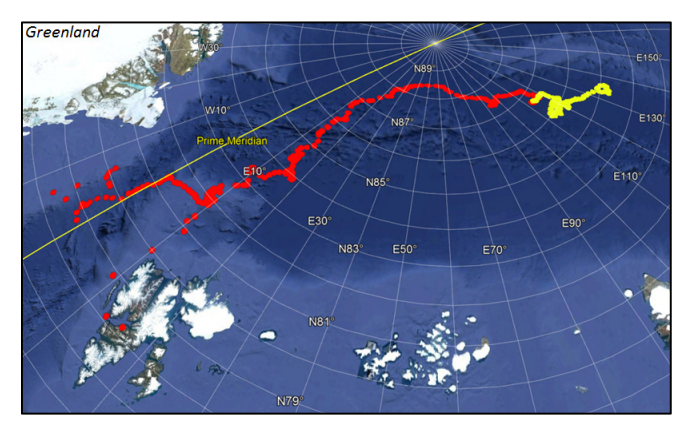


Fig. 1. Drift trajectory of the MOSAiC sea ice floe from October 2019 to September 2020. The yellow section indicates the drift during Leg 1.



Fig. 2. (Top) Ice lead developing next to the UWBRAD at the first RS-1 site. (Bottom) RS-2 site showing RS instruments including UWBRAD. (Photographs: Stefan Hendricks.)

The first RS site (RS-1) was established on October 18 with the RS instruments aligned to monitor undeformed secondyear ice with a fraction of refrozen melt ponds, which was typical for the southern parts of the ice floe. UWBRAD was installed at RS-1 on November 1 and started initial checkout measurements during this time (Fig. 2). The measured ice thickness at RS-1 at the beginning of November was 55–65 cm for the monitored region, but the instruments were positioned on surrounding ridged areas with thicknesses up to 2 m. The measured snow depth was around 5-15 cm. On November 16, several new ice cracks or leads were observed at the site and all instruments were retreated to safer locations. At this point, UWBRAD had not completed initial checkout testing, so the sea ice microwave emissions from the RS-1 site could not be observed. The deformation of the ice floe continued for about a week, and the establishment of another RS site was delayed until the floe stabilized and the recently formed cracks/leads were sufficiently frozen.

TABLE I		
UWBRAD INSTRUMENT SPECIFICATIONS [	311	

Frequency	~88 MHz bandwidth channels at center
	frequencies: 540, 900, 1380, 1740 MHz
Polarization	Single (Right-hand circular)
Observation Angle	Elevation (0° - 180°) and Azimuth (0° - 90°)
Platform Height	Min: 2 m , Max: 5 m
Ant. Gain (dB)/Beamwidth	11 dB / 60°
Calibration (Internal)	Reference load and noise diode
Calibration (External)	Sky Measurements
Integration time	100 msec
Noise equiv dT	1 K in 100 msec (each 88 MHz channel)
Interference	Full sampling of bandwidth in 16 bits resolution
Management	each channel; real time "software defined"
	RFI detection and mitigation

A second RS site (RS-2) having similar snow and ice characteristics was established on November 29 after relocating the instruments (Fig. 2). At the beginning of December, an average ice thickness of 70–80 cm and snow depth of 15–20 cm were observed at RS-2; the snow depth increased to 20–25 cm in subsequent days. UWBRAD was redeployed at this site on December 3 and performed measurements from December 4 to 13. The formation of new cracks in the area on December 13 ended UWBRAD measurements during Leg 1. Additional datasets (not described in this article) were obtained during Leg 2 and will be reported in future publications.

# B. UWBRAD Instrument Characteristics

UWBRAD was originally developed to observe circularly polarized TBs in multiple independent channels over the 0.5–2 GHz range. A right-handed circularly polarized (RHCP) conical spiral antenna having a beamwidth of ~60° that remains uniform over the operating frequency range is used. For the MOSAiC campaign, the instrument performed observations in four frequency channels (540, 900, 1380, and 1740 MHz). Since the instrument operates over a frequency range outside traditional protected bands, it uses real-time algorithms to detect and filter RFI. Table I summarizes the main instrument specifications.

Each channel has an ~88 MHz bandwidth that is further resolved into 0.24-MHz sub-bands both to facilitate RFI removal and to observe TB characteristics versus frequency. The acquired spectra are reported as 100-ms integration time data products that are further resolved at 1-ms intervals. In addition, full-band products representing the total power in each channel, and its kurtosis are also reported at 1-ms resolution. The instrument filters the measured TB spectrograms through pulse-blanking and kurtosis detection algorithms and performs additional temporal integrations to produce "medium rate" data products every ~3.5 s. This rate is sufficient given the relatively slow evolution of sea ice and snow at the RS-2 site. The medium rate data are processed further after the campaign in order to detect and discard any remaining RFI

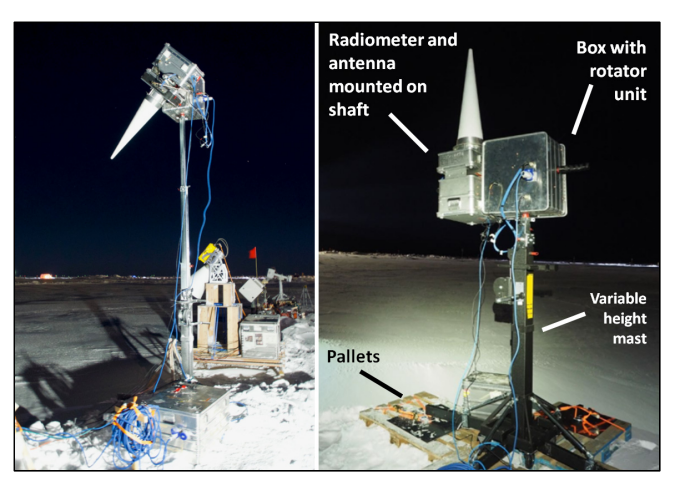


Fig. 3. (Left) UWBRAD observes sea ice emissions at the RS-2 site. (Right) The instrument at the RS-1 site in its sky measurement configuration. (Photographs: Gunnar Spreen.)

through longer term pulse blanking, spectral kurtosis, and cross-frequency algorithms [39], [40].

The instrument was deployed on a stationary telescoping mast that can be manually adjusted to different heights when needed (Fig. 3). The elevation angle of the antenna was controlled by a programmable rotator unit which allowed it both to monitor sea ice from a desired oblique angle and to perform periodic upward looking sky measurements for calibration. No azimuth rotation of the antenna was performed after installation.

# C. Calibration

UWBRAD internal calibration process, as described in [32], is applied here for the four frequency channels and observation cycles of  $\sim$ 3.5 s. For calibration, the data from four different radiometer states is recorded: antenna, antenna plus noise diode, reference load, and reference plus noise diode. The physical temperature of reference load is recorded internally, and laboratory tests prior to installation with a liquid nitrogen cooled termination were used to characterize the noise diode excess brightness. These measurements and information allow the calibration of UWBRAD antenna measurements into the antenna noise temperature in Kelvin. The TB of the scene is then estimated through external calibration performed using the periodic sky measurements recorded. The instrument was designed to automatically direct its antenna toward zenith for 5 of every 15 min (Fig. 4). The antenna loss was estimated over 1-h-long windows by using the sky observations over this time interval along with the antenna physical temperature.

### D. Calibrated Brightness Temperatures

Fig. 5 provides example spectrograms before external calibration and final RFI processing (upper) and after external calibration and final RFI processing (lower) for measurements on December 9. The final RFI processing was found to eliminate a large portion of the spectrum due to apparent self-emission from the UWBRAD computer, since external RFI was not substantially present at the measurement location.

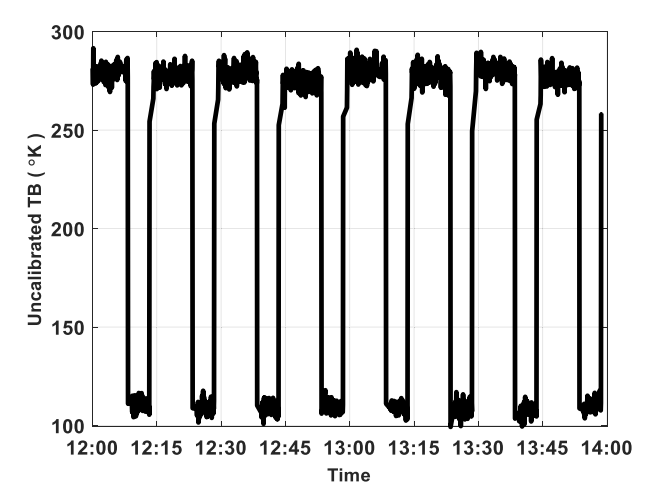


Fig. 4. 1380-MHz antenna temperature time series showing sea ice and sky observations. The measured radiation from sea ice is calibrated with respect to the weak sky radiation over 1-h long time periods.

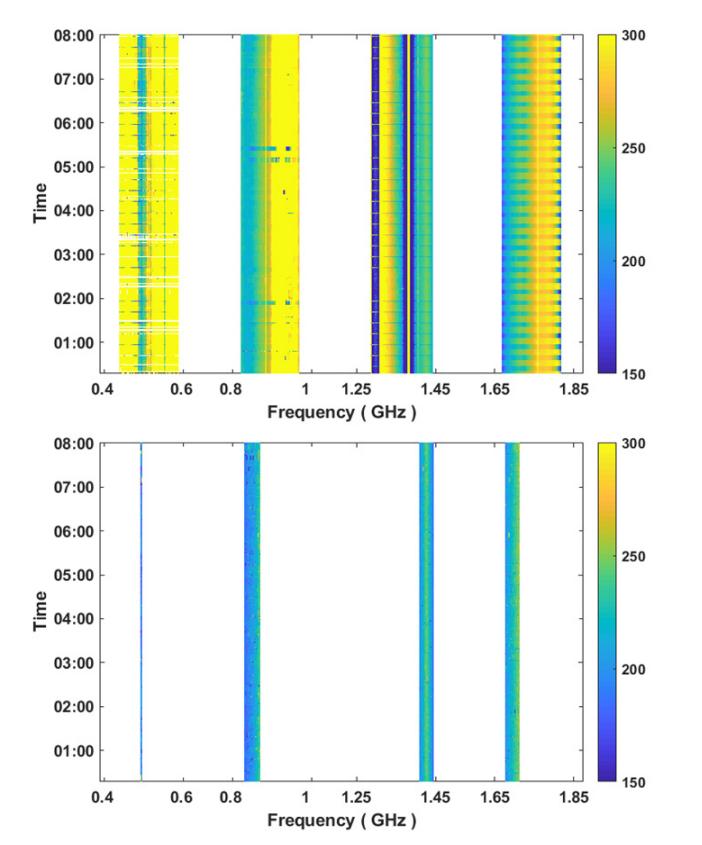


Fig. 5. Brightness temperature (K) spectrograms from observations on December 9 (top) before and (bottom) after calibration and RFI mitigation.

This interference mostly impacts the lowest frequency channel (540 MHz) resulting in only a narrow bandwidth remaining and increased uncertainty in this channel's measurements. TB time series were then obtained by integrating over the remaining spectra of each channel (see Fig. 6). Each data point on the plot corresponds to an effective TB from a 6-min-long observation which was obtained by averaging the original data over windows of 100 samples.

The instrument started its automatic measurements at RS-2 on December 4 and finished its observations on

December 13 when cracks in the ice developed at RS-2. The measurements were interrupted on December 10 due to a disconnection of the computer's power cable, but were restored the next day. Larger step changes in observed TBs correspond to differing antenna pointing angles (35°, 40°, 45°, and 50° as shown in the lower panel in Fig. 6) that were selected throughout the observations. In the second half of the measurement period, the orientation was kept at 35° to observe the impact of ice growth on the TB as a continuous time series at a fixed elevation angle.

As a result of increased internal RFI, measurements from the 540-MHz channel are missing after December 11, and significant variability is observed in this channel over the entire time series. Measurements at 900 and 1380 MHz are more stable, but also show apparent RFI impacts that cause deviations up to 8 K especially on December 12. The 1740-MHz measurements show some anomalous variability on December 8 and 10, but otherwise appear stable. All channels except 540 MHz show a gradual increase in TB after December 8 that is attributed to the slow ice growth, as will be discussed in Section V. In addition, the increasing trend for channels 900 and 1380 MHz is ceased by a small drop in the TB at midnight on December 10. Sometime around this point, the instrument stopped sky measurements due to a software glitch; therefore, the sky measurements from the previous day were used for calibration of the data on December 10. This effect highlights the importance of frequent sky observations for calibration.

# III. MODELING

# A. Sea Ice Emissions

Arctic sea ice can be modeled as a combination of multiple layers representing snow and ice overlying the ocean. The resulting emissivity of sea ice then strongly depends on the electromagnetic properties of these layers. The sea ice region observed at the RS-2 site was covered with undisturbed dry snow. A mixing formula [42] was used to estimate the corresponding snow dielectric properties. The RS-2 site remained intact without any crack development despite the stormy weather and low air temperatures, and we do not expect significant changes in snow characteristics from December 4 to 13 except for the snow depth.

Sea ice dielectric properties for both first-year (FYI) and second-year (SYI) ice types are modeled based on their brine volume fraction according to the semiempirical results in [43]. Coefficients from this model were interpolated to fit to the frequency channels of interest. The relative brine volume for both types of ice is estimated from [44] which depend on the ice temperature and bulk salinity, both of which were obtained or interpreted from relevant *in-situ* measurements (ice cores and thermistor chains). We assume homogeneous ice and snow layers and neglect volume scattering, as air bubbles and brine pockets are much smaller than the wavelengths of interest [45].

From December 4 to 13, bulk ice dielectric characteristics were not expected to change significantly since the measurements were performed in the winter growth season. However, several centimeters of ice growing at the bottom was observed

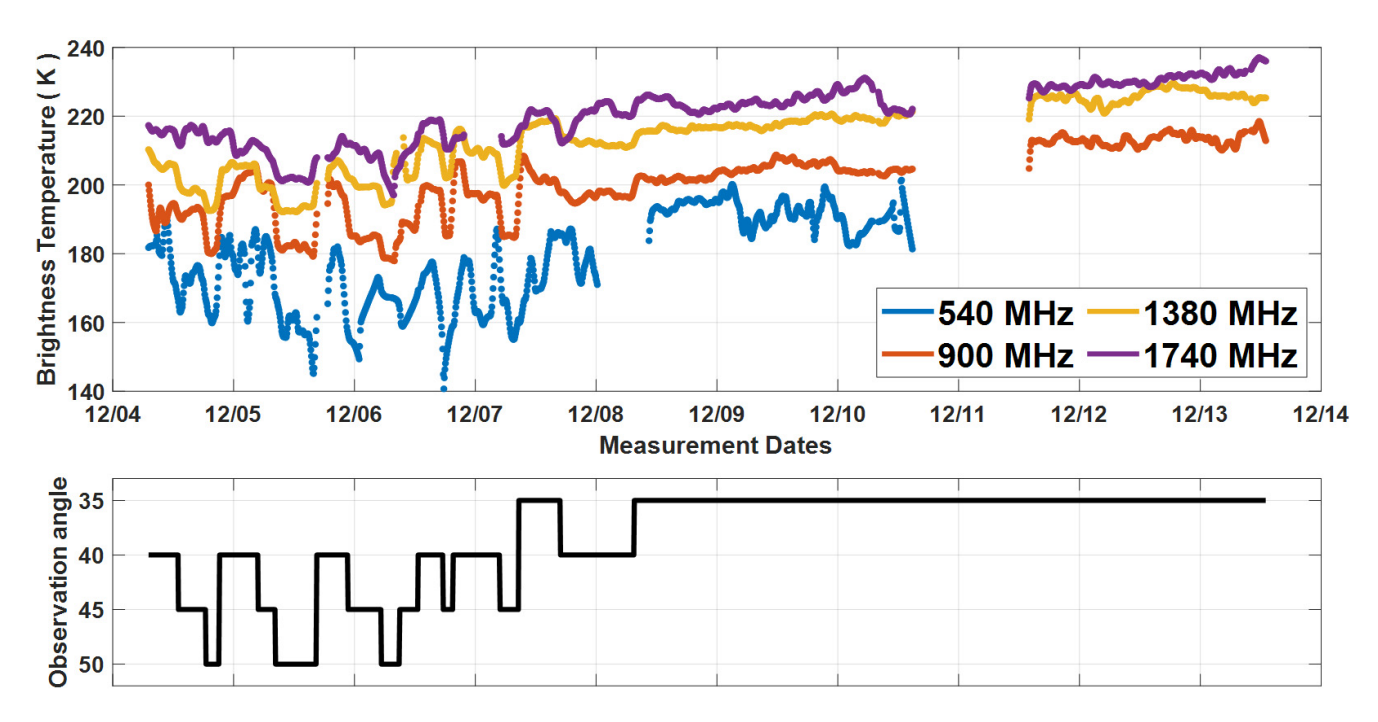


Fig. 6. Calibrated TB time series from (top) December 4 to December 13, and (bottom) corresponding off-nadir antenna angles [41].

at the site according to the thermistor chain data. Note that no measurements were conducted at RS-2 after the development of cracks on December 13.

The sea water permittivity was estimated from [46] with the salinity and temperature values of 31 (reported in dimensionless practical salinity,  $S_P$ ) and -1.8 °C, respectively, as measured from the sensors of the ship and from a thermistor chain at the RS-2 site. These values also did not vary significantly throughout the observation period.

## B. Radiative Transfer (RT) Model

Microwave brightness temperatures of sea ice were simulated through a modified incoherent radiative transfer (RT) model [47] for a planar layered medium. An incoherent model is appropriate because no coherent interference effects are expected due to the typical sea ice bottom interface roughness having rms height in the tens of centimeters and the  $\sim\!20$  m scale footprint. The model accounts for multiple reflections between layer interfaces, which may have significant contributions especially for low-loss desalinated ice layers.

The sea ice was separated into multiple layers through analysis of its salinity profile (obtained from ice cores) and internal temperature (obtained from thermistor chain measurements). The physical temperature of each layer was assumed to be the temperature measured by the thermistor chain in the middle of the layer. This assumption is not unrealistic given the near-linear temperature variation inside the ice and snow according to *in-situ* measurements at the observation site.

Cosmic and atmospheric radiation (estimated as a total of  $\sim$ 5 K [48], [49]) reflected from the ice floe surface and the dry snow emissions were also included. Because UWBRAD used an RHCP antenna, model predictions were taken as the average of the predicted horizontally and vertically polarized TBs. In addition, the antenna gain was projected over the

monitored ice surface for the averaging of the radiated signals incident to the antenna. For each antenna off-nadir angle at which the UWBRAD made measurements, this projection is recalculated to better model the observed thermal emissions.

# IV. ANCILLARY DATA

# A. Temperature Profile

Ice temperature is a critical parameter in the model as it impacts the brine volume and changes the ice electromagnetic properties. Warmer ice typically has larger permittivity and attenuation which leads to lower emissivity and the isolation of lower layers. Given that the ice temperature reacts to the continuously fluctuating air temperature with a thermodynamic delay, it is important to determine this parameter with high accuracy so that meaningful interpretations can be made.

During the expedition, digital thermistor chains (DTCs) were installed at numerous locations on the ice floe. One of these units was placed at and near ( $\sim$ 200 m away from) the RS-2 site so that the vertical temperature profiles of snow and ice could be sampled at a vertical resolution of 2 cm. These DTC units (DTC\_20 and DTC\_22) acquired measurements every hour which is sufficiently frequent to follow the slow temperature change in the snow-covered ice (Fig. 7). The time series of measured air temperatures show substantial variations starting around -15 °C and ending around -21 °C. The ice surface temperature follows a similar trend but with reduced variability. The difference between these two quantities stems from the thermal insulation of the snow cover, and the temperature difference reaches up to 17 °C on December 12. Since the ocean temperature remained constant at the freezing point  $(-1.8 \, ^{\circ}\text{C})$ , temperature deeper in the ice fluctuate more slowly, although even a 1 °C change can impact TBs for low-salinity ice.

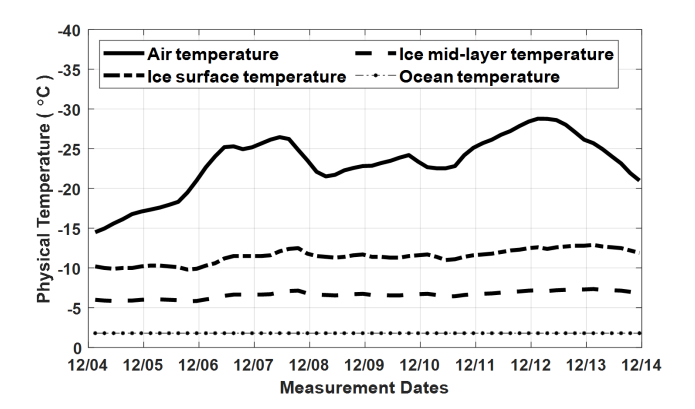


Fig. 7. Time series of the sea ice temperature profile obtained from the fusion of data collected by the thermistor chains DTC\_20 (near the RS-2) and DTC\_22 (at the RS-2) [50].

The snow temperature is taken as the average of the air and ice surface temperatures. The error from this assumption is not expected to be significant given the small emission contributions from the snow layer in general due to its very low loss at the frequencies of interest.

### B. Salinity Profile

Together with the temperature, salinity affects the relative brine volume fraction in the sea ice body and thus its thermal radiation. Bulk sea ice salinity is difficult to determine remotely and its profile is not necessarily constant or linear. As a consequence, accurate knowledge of sea ice salinity is important in modeling sea ice TBs.

Throughout the expedition, sea ice cores were taken from multiple locations on the ice floe for detailed examination of properties including salinity. Sampling activities typically occurred weekly except during storm periods. Some of the ice cores obtained during the expedition were extracted from SYI on the same floe, which are likely made of remnant ice that survived at least one summer melt season [51]. Salinity profiles measured at the SYI coring sites showed consistent ice characteristics from October to December. The stratigraphy consists of a remnant second-year layer on top which survived a summer melt and therefore is desalinated with salinity values  $S_P \sim 0.4$ . The new ice underneath formed as a first-year layer which grew up to 15-cm thickness (at the time of our observations) with an average  $S_P$  of  $\sim$ 5, similar to the SYI characteristics observed in [52].

Although it is a common approach to assume a single bulk sea ice salinity in emission modeling, the SYI of MOSAiC is made of two layers with different characteristics that should be taken into account in the model. In particular, the presence of a more saline layer below a low-salinity layer can significantly change the predicted thermal emission. This impact is even larger for SYI with a thinner desalinated second-year layer at the top. In addition, the continuous growth of the first-year layer can eventually allow it to dominate the electromagnetic response of the SYI. Therefore, this first-year layer was included in the model to investigate its impact on TB.

The SYI ice coring locations were more than 500 m away from the RS-2 site. Early evidence (such as the initial location

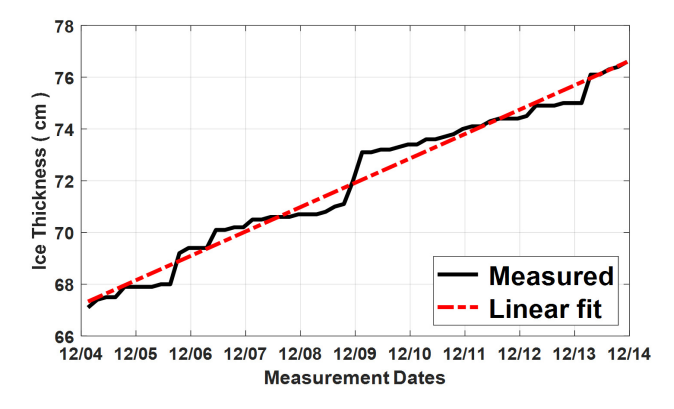


Fig. 8. Sea ice thickness growth during the operation of the UWBRAD. The data was extracted from readings of the DTC installed at the RS-2.

of RS-2 on the floe prior to displacement due to the storm event, surface topography, and ice thickness) suggests that the RS-2 site is likely to have refrozen melt ponds. The absence of thin section stratigraphy at the RS-2 site does not allow us to differentiate conclusively between the two ice types (SYI or refrozen melt pond). However, the salinity of refrozen melt ponds formed over remnant ice is known to be low [53], [54], and with the new ice growing underneath, the RS-2 site may reasonably be expected to have a salinity profile similar to the SYI at the coring site. In addition, the initial thickness measured at the RS-2 site matches one of the second-year layer thicknesses of the SYI site. Due to their low salinity, desalinated remnant ice and refrozen melt ponds are likely to behave similarly from a dielectric perspective. Therefore, the presence of either ice type at the RS-2 site is not expected to significantly impact the RT model developed in this study.

# C. Ice Thickness and Snow Depth

Ice thickness is also an important factor impacting sea ice thermal emission. Even small thickness variations can manifest as a significant increase in the observed TBs depending on the characteristics of the ice. Therefore, continuous *in-situ* measurements of ice thickness were critical.

For an approximation of the ice thickness, ice core samples taken from the representative sites are useful. However, their sampling frequency was low, and ice cores were not extracted at the RS-2 site leading to a loss of fine-scale information on ice growth. To address this problem, temperature profile data from DTCs that were deployed at and near the RS-2 site were utilized to determine ice thickness.

The extracted sea ice thickness information from DTCs that were installed both on undeformed ice at the RS-2 (DTC\_22) and on the transect line nearby (DTC\_20) shows that there is about 8.3 cm of new ice growth during UWBRAD operation (Fig. 8). The sea ice gradually grows from 67.8 cm on December 4 and reaches 76.1 cm on December 13. Small jumps in the recorded thickness are due to the resolution limit of the DTCs in which it becomes difficult to determine the exact thickness if the ocean–ice boundary lies between two consecutive thermistors on the chain. A linear fit to the extracted data is also shown.

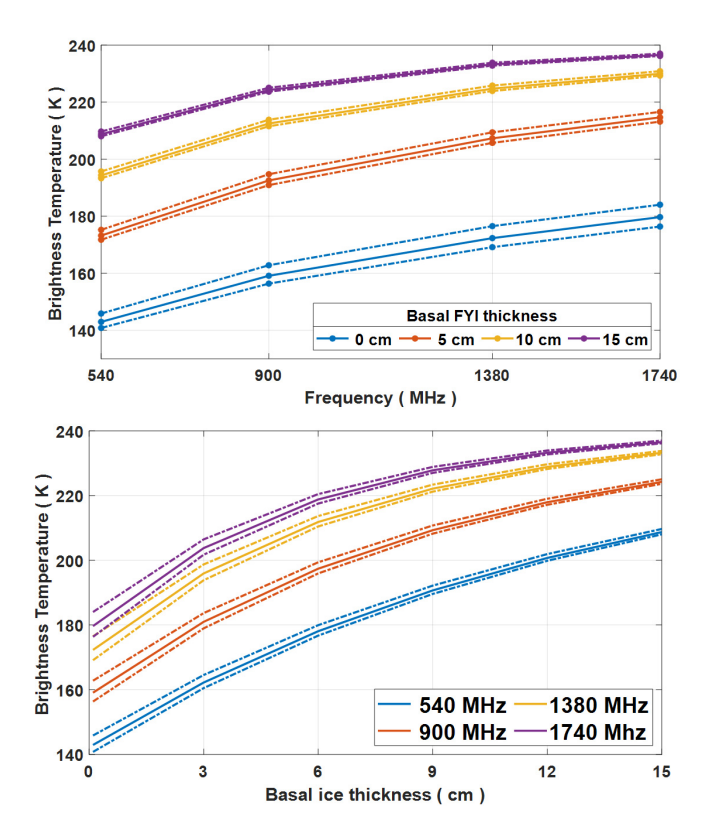


Fig. 9. Effect of a first-year layer on the observed thermal radiation at 35° off-nadir incidence angle is demonstrated with (top) TB versus frequency and (bottom) TB versus basal FYI thickness plots. The sea ice characteristics used in the simulations are given in Table II. The dashed lines represent the effect of 0.5 °C physical temperature margins of second-year layer as shown in Table II.

The thermal emission from dry snow is small at low microwave frequencies since it has negligible attenuation. However, it still impacts both the ice temperature and the refraction of sea ice emissions. Snow depth was measured with a snow gauge at multiple spots in the vicinity of UWBRAD on December 12. The measured snow depth next to the deployed instruments ranged between 8 and 35 cm with an average of 15 cm. The spatial variations were due to the recent storm which led to significant drift and formation of snow dunes. An average value of 15 cm is used in the forward model. Since the snow at RS-2 site was not sampled during the operation of the UWBRAD, its density was assumed 0.35 g/cm³ in TB simulations. Despite the lack of data on this parameter, snow layer properties do not significantly impact the modeled TB values.

# V. RESULTS

# A. Model Simulations

The final model represented sea ice as a three-layer structure, composed of one snow layer on top of two ice layers (the remnant desalinated second-year layer on top of a new more saline first-year layer) above the ocean half-space. Material properties are as specified in Table II. Results for 35° off-nadir angle are shown in Fig. 9 and show an increasing TB with frequency. This is an expected feature since electromagnetic loss in sea ice is lower at lower frequencies, for which the ice is more transparent and the "colder" ocean returns are

TABLE II

CHARACTERISTICS OF LAYERS FOR SIMULATING THE MICROWAVE RADIATION EXPECTED TO BE OBSERVED AT RS-2. AVERAGE LAYER TEMPERATURES AND SALINITIES USED ARE IN THIS TABLE

	Thickness (cm)	Salinity (psu)	Temperature (°C)	Snow Density (g/cm³)	
Snow	15	-	-15.0	0.35	
Second-year Layer	63	0.4	-6.0 ± 0.5	-	
First-year Layer	0 - 15	5	-2.3	-	
Ocean	-	31	-1.8	-	

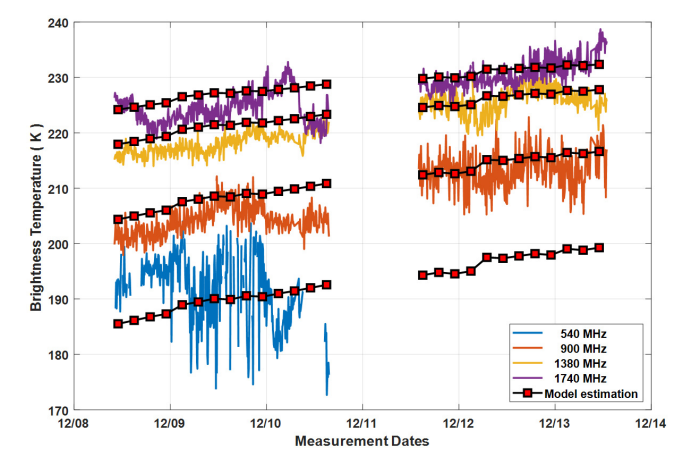


Fig. 10. Comparison of the measured and modeled TB time series for the period when the antenna orientation was kept at  $35^{\circ}$  off-nadir. The model predicts a gradual increase of  $\sim 10$  K for all channels.

more evident. The variation in TBs with frequency can provide additional information on ice characteristics as compared to a single-frequency channel observation; this is one of the main motivations for using UWBRAD for the retrieval of sea ice properties [33]. The TBs of all channels significantly increase with the growth of the first-year layer. This bottom layer has a strong impact despite its smaller thickness due to its larger electromagnetic loss, emission, and attenuation. The low-frequency channel is more sensitive to this bottom growth compared to the other ones because the 540-MHz signals are less impacted by attenuation in the second-year layer. For the same reason, the highest frequency channel tends to show saturation after the first-year layer thickness exceeds ~9 cm.

It can also be observed that the TBs do not show a strong correlation to the variation in average temperature in the second-year layer (bottom plot in Fig. 9) due to the dominating effect of the first-year layer. Note that it is assumed in this simulation that the first-year layer shows negligible variations in its average temperature since it is just above the ocean surface and is relatively thin.

# B. Comparison With the Measured Data

The availability of *in-situ* data provides the opportunity to directly compare measured and modeled TBs. In this process, model predictions were obtained for the UWBRAD antenna pointing angle at a specific time and using the temperature and

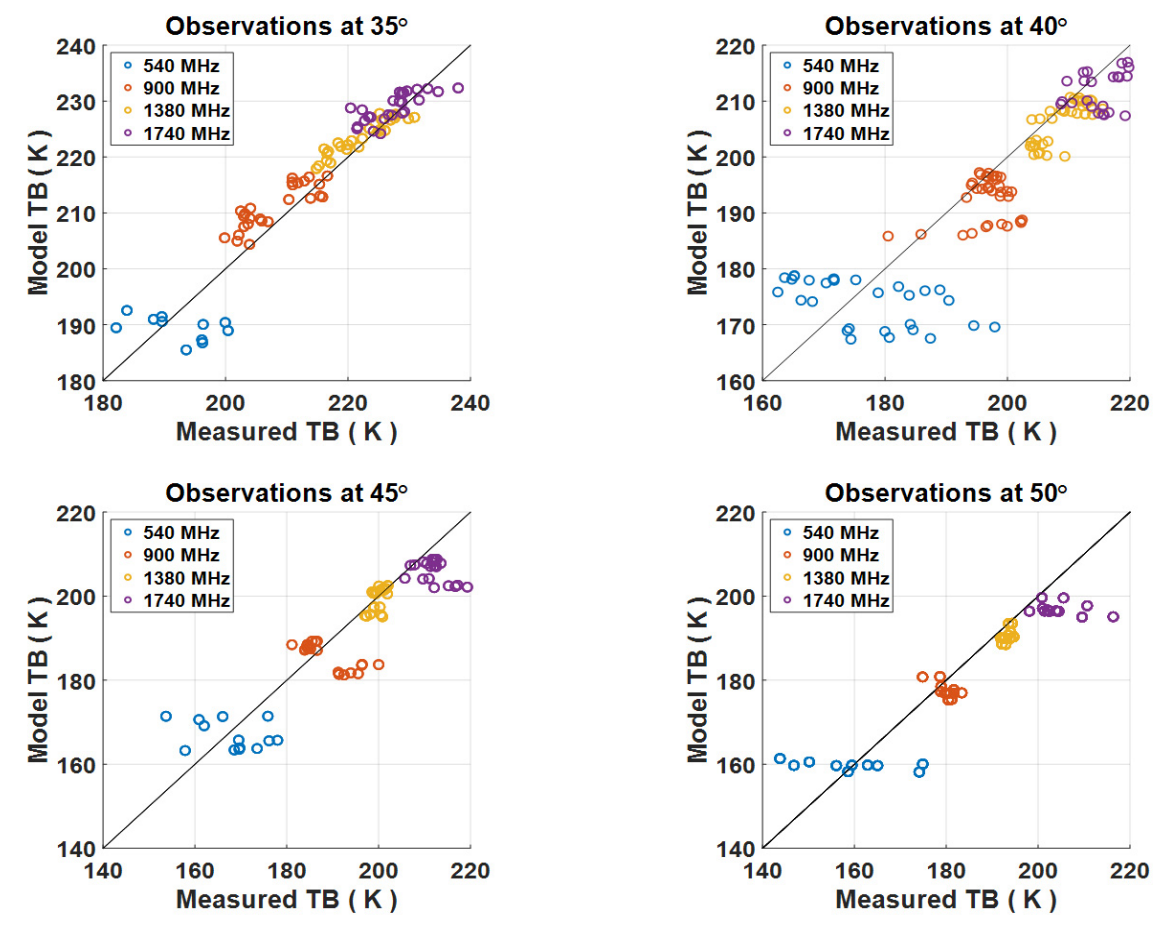


Fig. 11. Scatterplots of the measured and modeled TB time series for the off-nadir observation angles 35°, 40°, 45°, and 50°, respectively. All channels show low standard errors except the channel 540 MHz due to intense internal RFI. Scatterplot sampling period is approximately 6 h for 35° observation angle, and 1 h for the rest over the time periods shown in Fig. 6 for each observation angle.

ice property in-situ time series. Because the exact thickness of the growing first-year layer was not available as a time series and could not be inferred from thermistor chain data alone, bottom layer thickness values between 0 and 15 cm were tested to compare the simulated and observed TBs over the time period of December 8–13 (at fixed 35° pointing angle). The best fit values were determined as 8.7 cm on December 9 and 13.5 cm on December 13, both of which are in the range of first-year layer thicknesses detected in ice core samples taken from representative sites. Fig. 10 presents the resulting comparison of measured and modeled TB time series during this time interval; the high variability at 540 MHz is again apparent, but otherwise reasonable agreement is observed. The upper left Fig. 11 further presents a scatter plot of the measured and modeled TBs over the December 8-13 time series. The results again show a reasonable agreement between measurements of the model predictions over the frequency range and ice conditions examined. It is noted that the ice physical temperature drops 1 °C on average between December 8 and December 13 according to the DTC readings, but the increased TBs caused by the growth of the first-year layer remain apparent.

The corresponding first-year layer thickness values were estimated for December 4–8 based on the ice growth data from the DTCs, resulting in the layer thickness increasing from 5.2 to 8.7 cm during this time period. Datasets during this

TABLE III

ABSOLUTE BIAS AND ROOT-MEAN-SQUARE DEVIATION (RMSD)

VALUES OF THE SCATTERPLOTS DEPICTED IN FIG. 11

Bias  (°K)				RMSD (°K)						
	540	900	1380	1740	Γ		540	900	1380	1740
	MHz	MHz	MHz	MHz	L		MHz	MHz	MHz	MHz
35°	1.7	3.0	1.2	1.3		35°	8.1	4.2	2.6	3.2
40°	1.6	4.1	2.6	5.1		40°	12.9	6.2	3.6	7.0
45°	2.3	3.1	0.6	6.0		45°	12.3	8.6	2.3	7.8
50°	1.7	1.9	2.3	7.3		50°	10.5	4.2	3.1	9.5

time period provide the results shown in Fig. 11 at varying antenna pointing angles. Although there is high variability at 540 MHz, a reasonable match between measured data and model predictions is again observed. The corresponding bias and RMSD values for these scatterplots are also listed in Table III.

The results demonstrate the significance of including the more saline first-year layer at the bottom of SYI in the emission model. If the whole ice body were instead assumed to be desalinated sea ice with  $S_P$  of 0.4, it would not be possible to achieve good agreement between the model and the measurements. This also indicates that the proposed sea ice stratigraphy model (remnant second-year and growing first-year ice) provides a useful tool for predicting thermal emission from a remnant or refrozen melt pond during the winter freeze-up season. We also note that if these are dominant

ice types for the level parts of the MOSAiC floe (which will be determined after further investigations), these findings can be relevant also for interpreting the data of other RS measurements at this site.

#### C. Discussion

Although sea ice is assumed to have planar boundaries in the model, in reality, the sea ice bottom and surfaces can have a substantial roughness. During the instrument installation, the RS-2 measurement site was undeformed second-year ice, and both the snow and ice surface topographies were flat based on both the visible observations and airborne laser scanner images. Therefore, a planar surface should be a reasonable approximation at the microwave frequencies of interest. Information on the roughness of the bottom layer is not currently available, but is being investigated based on other measurements in the campaign. The impact of this roughness remains uncertain, although bottom roughness effects are typically neglected in existing sea ice retrieval strategies using 1400-MHz measurements.

Additional uncertainty is introduced by the saline first-year layer defined in the emission model and the requirement to determine its exact thickness based on a correlation with measured data. This was necessary due to the lack of ice core samples at the RS-2 site; nevertheless, the range of values used through the matchup process appears reasonable compared to existing information from ice cores in the area.

UWBRAD antenna footprint also covered an elliptical area of  $\sim 10 \times 30 \text{ m}^2$  for antenna pointing angle 35° and a larger area for larger pointing angles. Any spatial inhomogeneities within this footprint (e.g., in ice thickness, ice bottom surface roughness, or salinity profile) therefore also can impact the obtained results. The impact of these effects remains a subject of investigation.

## VI. CONCLUSION

The 540–1740 MHz brightness temperatures of a drifting sea ice floe in the Arctic were successfully measured during the first leg of the MOSAiC expedition. The monitored site showed the characteristics of undeformed desalinated second-year ice (potentially with refrozen melt ponds). Observed TBs from this site were compared with the sea ice emission model using *in-situ* data of ice salinity and temperature. The comparison demonstrates the impact of new ice growing under the remnant ice on the observed TBs. An ice growth of about 8 cm was observed during the ten days of observation that resulted in a gradual increase in the TBs.

The results show the success of 540–1740 MHz microwave radiometry in measuring sea ice properties, particularly the varying sensitivities to ice properties with depth obtained through the use of multiple frequencies. In particular, saturation in the higher frequency channels was observed as the thickness of the first-year layer (and overall sea ice) increased that was not observed in lower frequency channels. These results motivate continued development of microwave radiometry from 0.5 to 2 GHz for observing sea ice properties.

Finally, while the results obtained provide a useful validation of models for predicting 0.5–2 GHz emission effects, the requirement for an inhomogeneous ice profile does not

necessarily indicate a similar requirement for space-borne seaice TB measurements. This is due to the significant differences in the spatial scales observed (here, tens of meters versus the tens of km used for space-borne L-band measurements) with the much coarser observations for space-borne systems representing a spatial average over many ice conditions (e.g., combinations of refrozen melt ponds and other more homogeneous ice). Analyses to investigate the potential performance of 0.5–2 GHz microwave radiometry for sea ice sensing over both smaller and larger spatial scales will continue toward the application of these technologies in space [55], [56].

#### ACKNOWLEDGMENT

The data used in this article was produced as part of the international Multidisciplinary drifting Observatory for the Study of the Arctic Climate (MOSAiC) with the tag MOSAiC20192020 and project ID AWI\_PS122\_00. The authors would like to thank the ice coring team members for their efforts throughout the leg 1 of the expedition.

## REFERENCES

- [1] W. N. Meier et al., "Arctic sea ice in transformation: A review of recent observed changes and impacts on biology and human activity," Rev. Geophys., vol. 52, pp. 185–217, Sep. 2014, doi: 10.1002/2013RG000431.2014.
- [2] R. Lindsay and A. Schweiger, "Arctic sea ice thickness loss determined using subsurface, aircraft, and satellite observations," *Cryosphere*, vol. 9, no. 1, pp. 269–283, Feb. 2015, doi: 10.5194/tc-9-269-2015.
- [3] A. H. H. Renner et al., "Evidence of Arctic sea ice thinning from direct observations," Geophys. Res. Lett., vol. 41, no. 14, pp. 5029–5036, 2014, doi: 10.1002/2014gl060369.
- [4] T. F. Stocker *et al.*, "Climate change 2013: The physical science basis," IPCC, Cambridge, U.K., Tech. Rep., 2013, p. 1535.
- [5] D. Cavalieri, C. L. Parkinson, P. Gloersen, and H. J. Zwally, "Sea ice concentrations from Nimbus-7 SMMR and DMSP SSM/I-SSMIS passive microwave data, version 1. (Updated yearly)," NASA Nat. Snow Ice Data Center Distrib. Act. Arch., Boulder, CO, USA, 1996, doi: 10.5067/8GQ8LZQVL0VL.
- [6] S. Martin, "Improvements in the estimates of ice thickness and production in the Chukchi sea polynyas derived from AMSR-E," Geophys. Res. Lett., vol. 32, no. 5, Mar. 2005, Art. no. L05505, doi: 10.1029/2004GL022013.
- [7] T. Tamura, K. I. Ohshima, T. Markus, D. J. Cavalieri, S. Nihashi, and N. Hirasawa, "Estimation of thin ice thickness and detection of fast ice from SSM/I data in the Antarctic Ocean," J. Atmos. Ocean. Technol., vol. 24, no. 10, pp. 1757–1772, Oct. 2007, doi: 10.1175/JTECH2113.1.
- [8] S. Nihashi, K. I. Ohshima, T. Tamura, Y. Fukamachi, and S.-I. Saitoh, "Thickness and production of sea ice in the Okhotsk sea coastal polynyas from AMSR-E," *J. Geophys. Res.*, vol. 114, Oct. 2009, Art. no. C10025, doi: 10.1029/2008JC005222.
- [9] R. K. Singh, S. R. Oza, N. K. Vyas, and A. Sarkar, "Estimation of thin ice thickness from the advanced microwave scanning radiometer-EOS for coastal polynyas in the Chukchi and Beaufort Seas," *IEEE Trans. Geosci. Remote Sen.*, vol. 49, no. 8, pp. 2993–2998, Aug. 2011.
- [10] G. Spreen, L. Kaleschke, and G. Heygster, "Sea ice remote sensing using AMSR-E 89-GHz channels," J. Geophys. Res., vol. 113, Feb. 2008, Art. no. C02S03, doi: 10.1029/2005JC003384.
- [11] R. Kwok, J. C. Curlander, R. McConnell, and S. S. Pang, "An ice-motion tracking system at the Alaska SAR facility," *IEEE J. Ocean. Eng.*, vol. 15, no. 1, pp. 44–54, Jan. 1990, doi: 10.1109/48.46835.
- [12] R. Ressel, S. Singha, S. Lehner, A. Rösel, and G. Spreen, "Investigation into different polarimetric features for sea ice classification using Xband synthetic aperture radar," *IEEE J. Sel. Topics Appl. Earth Observ. Remote Sens.*, vol. 9, no. 7, pp. 3131–3143, Jul. 2016.
- [13] N. Zakhvatkina, V. Smirnov, and I. Bychkova, "Satellite SAR data-based sea ice classification: An overview," *Geosciences*, vol. 9, no. 4, p. 152, Mar. 2019
- [14] Y. Yu and D. A. Rothrock, "Thin ice thickness from satellite thermal imagery," J. Geophys. Res., vol. 101, no. C11, pp. 25753–25766, Nov. 1996.

- [15] X. Wang, J. R. Key, and Y. Liu, "A thermodynamic model for estimating sea and lake ice thickness with optical satellite data," *J. Geophys. Res.*, vol. 115, Dec. 2010, Art. no. C12035, doi: 10.1029/2009JC005857.
- [16] M. Mäkynen, B. Cheng, and M. Similä, "On the accuracy of thinice thickness retrieval using MODIS thermal imagery over Arctic first-year ice," *Ann. Glaciol.*, vol. 54, no. 62, pp. 87–96, 2013, doi: 10.3189/2013AoG62A166.
- [17] R. Kwok and G. F. Cunningham, "Variability of Arctic sea ice thickness and volume from CryoSat-2," *Phil. Trans. Roy. Soc. A, Math.*, *Phys. Eng. Sci.*, vol. 373, no. 2045, Jul. 2015, Art. no. 20140157, doi: 10.1098/rsta.2014.0157.
- [18] S. W. Laxon et al., "CryoSat-2 estimates of Arctic sea ice thickness and volume," Geophys. Res. Lett., vol. 40, no. 4, pp. 732–737, Feb. 2013, doi: 10.1002/grl.50193.
- [19] S. Laxon, N. Peacock, and D. Smith, "High interannual variability of sea ice thickness in the Arctic region," *Nature*, vol. 425, no. 6961, pp. 947–950, 2003.
- [20] R. Kwok and G. F. Cunningham, "ICESat over Arctic sea ice: Estimation of snow depth and ice thickness," *J. Geophys. Res.*, vol. 113, no. C8, Aug. 2008, Art. no. C08010, doi: 10.1029/2008JC004753.
- [21] A. Schmitt and L. Kaleschke, "A consistent combination of brightness temperatures from SMOS and SMAP over polar oceans for sea ice applications," *Remote Sens.*, vol. 10, no. 4, p. 553, Apr. 2018.
  [22] N. Maaß, L. Kaleschke, X. Tian-Kunze, and M. Drusch, "Snow thick-
- [22] N. Maaß, L. Kaleschke, X. Tian-Kunze, and M. Drusch, "Snow thickness retrieval over thick Arctic sea ice using SMOS satellite data," *Cryosphere*, vol. 7, no. 6, pp. 1971–1989, Dec. 2013.
- [23] X. Tian-Kunze *et al.*, "SMOS-derived thin sea ice thickness: Algorithm baseline, product specifications and initial verification," *Cryosphere*, vol. 8, no. 3, pp. 997–1018, 2014.
- [24] L. Kaleschke, N. Maaß, C. Haas, S. Hendricks, G. Heygster, and R. Tonboe, "A sea-ice thickness retrieval model for 1.4 GHz radiometry and application to airborne measurements over low salinity sea-ice," *Cryosphere*, vol. 4, no. 4, pp. 583–592, 2010.
- [25] M. Huntemann, G. Heygster, L. Kaleschke, T. Krumpen, M. Mäkynen, and M. Drusch, "Empirical sea ice thickness retrieval during the freeze-up period from SMOS high incident angle observations," *Cryosphere*, vol. 8, no. 2, pp. 439–451, 2014.
- [26] C. Paţilea, G. Heygster, M. Huntemann, and G. Spreen, "Combined SMAP-SMOS thin sea ice thickness retrieval," *Cryosphere*, vol. 13, no. 2, pp. 675–691, Feb. 2019.
- [27] R. Ricker, S. Hendricks, L. Kaleschke, X. Tian-Kunze, J. King, and C. Haas, "A weekly Arctic sea-ice thickness data record from merged CryoSat-2 and SMOS satellite data," *Cryosphere*, vol. 11, pp. 1607–1623, Jul. 2017.
- [28] J. Menashi et al., "Low-frequency passive-microwave observations of sea-ice in the Weddell Sea," J. Geophys. Res, vol. 98, pp. 22569–22577, Dec. 1993.
- [29] M. T. Hallikainen, "A new low-salinity sea-ice model for UHF radiometry," Int. J. Remote Sens., vol. 4, no. 3, pp. 655–681, 2010.
- [30] J. T. Johnson et al., "The Ultra-Wideband Software-Defined Radiometer (UWBRAD) for ice sheet internal temperature sensing: Results from recent observations," in *Proc. IGARSS*, Jul. 2016, pp. 7085–7087.
- [31] M. J. Andrews et al., "The ultrawideband software-defined microwave radiometer: Instrument description and initial campaign results," *IEEE Trans. Geosci. Remote Sens.*, vol. 56, no. 10, pp. 5923–5935, Oct. 2018.
- [32] K. C. Jezek et al., "500–2000-MHz brightness temperature spectra of the northwestern Greenland ice sheet," IEEE Trans. Geosci. Remote Sens., vol. 56, no. 3, pp. 1485–1496, Mar. 2018, doi: 10.1109/TGRS.2017.2764381.
- [33] K. Jezek et al., "Remote sensing of sea ice thickness and Salinity with 0.5–2 GHz microwave radiometry," *IEEE Trans. Geosci. Remote Sensing*, vol. 57, no. 11, pp. 8672–8684, Jul. 2019.
- [34] M. Brogioni *et al.*, "500-2000-MHz airborne brightness temperature measurements over the East Antarctic Plateau," *IEEE Geosci. Remote Sens. Lett.*, early access, Feb. 17, 2021, doi: 10.1109/LGRS.2021.3056740.
- [35] MOSAiC (Multidisciplinary Drifting Observatory for the Study of Arctic Climate) Expedition. Accessed: Aug. 20, 2021. [Online]. Available: https://mosaic-expedition.org/
- [36] R. Knust, "Polar research and supply vessel POLARSTERN operated by the Alfred-Wegener-Institute," *J. Large-Scale Res. Facilities*, vol. 3, p. 119, Oct. 2017, doi: 10.17815/jlsrf-3-163.
- [37] T. Krumpen et al., "The MOSAiC ice floe: Sediment-laden survivor from the Siberian shelf," Cryosphere, vol. 14, no. 7, pp. 2173–2187, Jul. 2020.
- [38] G. Spreen *et al.* (2020). *Remote Sensing of Sea Ice on the MOSAiC Ice Floe*. AGU Fall Meeting. [Online]. Available: https://digital.csic.es/handle/10261/238294

- [39] M. J. Andrews, J. T. Johnson, M. Brogioni, G. Macelloni, and K. C. Jezek, "Properties of the 500-2000-MHz RFI environment observed in high-latitude airborne radiometer measurements," *IEEE Trans. Geosci. Remote Sens.*, early access, Jul. 8, 2021, doi: 10.1109/TGRS.2021.3090945.
- [40] M. Andrews et al., "P-band radiometry: RFI and calibration for uwbrad," in Proc. IEEE Int. Geosci. Remote Sens. Symp. (IGARSS), Waikoloa, HI, USA, Sep. 2020, pp. 6434–6437.
- [41] O. Demir and J. Johnson, "Arctic sea ice thermal emission measurements from the ultra wideband microwave radiometer (UWBRAD) at the multidisciplinary drifting observatory for the study of arctic climate (MOSAiC) expedition in December 2019," Arctic Data Center, 2021, doi: 10.18739/A23F4KP3J.
- [42] A. Sihvola, E. Nyfors, and M. Tiuri, "Mixing formulae and experimental results for the dielectric constant of snow," *J. Glaciol.*, vol. 31, no. 108, pp. 163–170, 1985.
- [43] M. Vant, R. O. Ramseier, and V. Makios, "The complex-dielectric constant of sea ice at frequencies in the range 0.1–40 GHz," J. Appl. Phys., vol. 49, no. 3, pp. 1264–1280, 1978.
- [44] G. Frankenstein and R. Garner, "Equations for determining the brine volume of sea ice from -0.5° to -22.9°C," *J. Glaciol.*, vol. 6, no. 48, pp. 943-944, 1967.
- [45] D. G. Barber *et al.*, "The role of snow on microwave emission and scattering over first-year sea ice," *IEEE Trans. Geosci. Remote Sens.*, vol. 36, no. 5, pp. 1750–1763, Sep. 1998.
- [46] L. Klein and C. Swift, "An improved model for the dielectric constant of sea water at microwave frequencies," *IEEE Trans. Antennas Propag.*, vol. AP-25, no. 1, pp. 104–111, Jan. 1977.
- [47] P. Mills and G. Heygster, "Sea ice emissivity modeling at L-band and application to 2007 pol-ice campaign field data," *IEEE Trans. Geosci. Remote Sens.*, vol. 49, no. 2, pp. 612–627, Feb. 2011.
- [48] J. D. Kraus, *Radio Astronomy*, 2nd ed. Powell, OH, USA: Cygnus-Quasar, 1986.
- [49] H. J. Liebe et al., "Propagation modeling of moist air and suspended water/ice particles at frequencies below 1000 GHz," in Proc. AGARD 52nd Spec. Meeting Electromagn. Wave Propag. Panel, 1993, Paper 542.
- [50] Sea Ice Temperature Data Collected by the Digital Thermistor Chains DTC\_20\_416 and DTC\_22\_416 at the Multidisciplinary Drifting Observatory for the Study of Arctic Climate (MOSAiC) Expedition in December 2019, PANGAEA, 2021.
- [51] M. Oggier et al. (2020). Ice core studies of autumn-to-spring sea ice evolution at the MOSAiC floe. AGU Fall Meeting. [Online]. Available: https://ui.adsabs.harvard.edu/abs/2020AGUFMC036...05O/abstract
- [52] M. A. Granskog et al., "Snow contribution to first-year and second-year Arctic sea ice mass balance north of svalbard," J. Geophys. Res., Oceans, vol. 122, no. 3, pp. 2539–2549, 2017.
- [53] D. K. Perovich et al., "Transpolar observations of the morphological properties of Arctic sea ice," J. Geophys. Res., vol. 114, Jan. 2009, Art. no. C00A04.
- [54] S. H. Lee *et al.*, "Holes in progressively thinning Arctic sea ice lead to new ice algae habitat," *Oceanography*, vol. 24, no. 3, pp. 302–308, Sep. 2011.
- [55] G. Macelloni et al., "Cryorad: A low frequency wideband radiometer mission for the study of the cryosphere," in Proc. IEEE Int. Geosci. Remote Sens. Symp. (IGARSS), Valencia, Spain, Jul. 2018, pp. 1998–2000
- [56] J. T. Johnson et al., "Microwave radiometry at frequencies from 500 to 1400 MHz: An emerging technology for Earth observations," IEEE J. Sel. Topics Appl. Earth Observ. Remote Sens., vol. 14, pp. 4894–4914, Apr. 2021, doi: 10.1109/JSTARS.2021.3073286.



Oguz Demir received the B.Sc. and M.Sc. degrees in electrical and electronics engineering from Middle East Technical University, Ankara, Turkey, in 2013 and 2017, respectively. He is pursuing the Ph.D. degree with the ElectroScience Laboratory, The Ohio State University, Columbus, OH, USA.

From 2013 to 2017, he was an RF/Microwave Engineer with Aselsan Inc., Ankara, where he was involved in designing microwave circuits for VHF/UHF radios and 4G/Long-Term-Evolution (LTE) base stations. He is a Graduate Research

Associate with the ElectroScience Laboratory, The Ohio State University. As part of his studies, he participated in the Multidisciplinary drifting Observatory for the Study of Arctic Climate (MOSAiC) expedition in 2019 to operate an ultra-wideband microwave radiometer to measure sea ice thermal emissions. His research interests include microwave remote sensing and ultra-wideband radiometry for sea ice observations.



Joel T. Johnson (Fellow, IEEE) received the Bachelor of Electrical Engineering degree from the Georgia Institute of Technology, Atlanta, GA, USA, in 1991, and the S.M. and Ph.D. degrees from the Massachusetts Institute of Technology, Cambridge, MI, USA, in 1993 and 1996, respectively.

He is a Burn and Sue Lin Professor with the Department of Electrical and Computer Engineering and ElectroScience Laboratory, The Ohio State University, Columbus, OH, USA. His research interests are in the areas of microwave remote sensing,

propagation, and electromagnetic wave theory.

Dr. Johnson is a member of commissions B and F of the International Union of Radio Science (URSI), and a member of Tau Beta Pi, Eta Kappa Nu, and Phi Kappa Phi. He received the 1993 Best Paper Award from the IEEE Geoscience and Remote Sensing Society, was named an Office of Naval Research Young Investigator, National Science Foundation Career awardee, and PECASE Award recipient in 1997, and was recognized by the U.S. National Committee of URSI as a Booker Fellow in 2002.



Kenneth C. Jezek received the B.S. degree in physics from the University of Illinois at Urbana–Champaign, Champaign, IL, USA, in 1973, and the M.S. and Ph.D. degrees in geophysics from the University of Wisconsin–Madison, Madison, WI, USA, in 1977 and 1980, respectively, with a focus on the behavior of the Ross Ice Shelf, Antarctica, using ice sounding radar data collected during several visits to the Antarctic.

He was the Manager of the NASA's Polar Oceans and Ice Sheets Program. He was a Geophysicist

with the U.S. Army Cold Regions Research and Engineering Laboratory, Hanover, NH, USA, where he was involved in the electromagnetic and acoustical properties of sea ice in the laboratory and in the Arctic. In 1989, he joined the Byrd Polar Research Center, School of Earth Sciences, The Ohio State University (OSU), Columbus, OH, USA, as the Director, where he is a Professor Emeritus. From 1997 to 2007, he led the Radarasat Antarctic Mapping Project. His research interests include application of ultrawideband radiometry to ice sheet and sea ice studies.

Dr. Jezek served as a Co-Leader for the International Polar Year GIIPSY Project that involved the participation of 12 space agencies from 2007 to 2010. He chaired the Land Ice Science Team for NASA's Operation Icebridge from 2010 to 2013. He has been serving on 13 NRC committees since 1989.



Mark J. Andrews (Member, IEEE) received the B.S. degree in electrical and computer engineering from The Ohio State University, Columbus, OH, USA, in 2008, and the M.S. degree in electrical engineering from the University of Southern California, Los Angeles, CA, USA, in 2011.

He is a Payload Systems Engineer with the Boeing Satellite Development Center, El Segundo, CA, USA.

In 2013, he returned to Columbus, OH, USA, as a Radar Systems Engineer with STAR Dynamics,

Hilliard, OH, USA. Beginning 2014, he has been a Research Associate with the OSU's ElectroScience Laboratory, focusing on radar and radiometry research while pursuing his Ph.D.

**Kenneth Ayotte**, photograph and biography not available at the time of publication.



**Gunnar Spreen** (Member, IEEE) received the M.Sc. degree in physics (Diplomphysiker) and the Ph.D. degree in oceanography from the University of Hamburg, Hamburg, Germany, in 2004 and 2008, respectively.

He works on satellite remote sensing of Polar Regions with a focus on monitoring changes of sea ice (extent, mass, and dynamics) and on understanding underlying climate processes. Satellite measurements are validated using ground-based and airborne field observations, recently in particular from the

2019/2020 Multidisciplinary drifting Observatory for the Study of Arctic Climate (MOSAiC) expedition. For which, he serves on the project board and coordinates the remote-sensing activities. He was a Research Scientist with the Norwegian Polar Institute, Tromsø, Norway, and a Post-Doctoral Scholar

with the Jet Propulsion Laboratory, California Institute of Technology, Pasadena, CA, USA. He is the Head of the research group "Remote Sensing of Polar Regions" at the University of Bremen, Institute of Environmental Physics, Bremen, Germany. His work addresses the development of new retrievals for sea ice parameters like leads and ice type from synthetic aperture radar (SAR) and microwave radiometer data as well as snow on sea ice.



**Stefan Hendricks** received the Ph.D. degree from the University of Bremen, Bremen, Germany, in 2009

Besides the Ph.D. program, he was a Project Scientist and nowadays as a Senior Scientist at the Sea Ice Physics Section, Alfred Wegener Institute, Helmholtz Centre for Polar and Marine Research, Bremerhaven, Germany. His research focus is the observation of global sea—ice thickness with geophysical methods and satellite remote sensing.



Lars Kaleschke received the M.Sc. and Ph.D. degrees in physics from the University of Bremen, Bremen, Germany, in 1998 and 2003, respectively.

From 2006 to 2018, he was a Professor with the Universität Hamburg's Institute of Oceanography, Hamburg, Germany, where he was involved in setting up the DFG Cluster of Excellence for climater research. There he headed the research topic Arctic Regions and Permafrost. He coordinated various research projects and was involved in developing and testing a system for ice prediction and route

optimization to facilitate safe and efficient navigation for ships operating in the ice. In 2019, he moved to the AWI and subsequently took part in the longest leg of Multidisciplinary drifting Observatory for the Study of Arctic Climate (MOSAiC), the largest expedition to the Central Arctic to date. The measurements he took on the sea ice using microwave radiometers are essential for the further development and validation of satellite-based methods used for comprehensive observation of the polar regions. He is an expert on remote sensing at the Sea Ice Physics Section of the Alfred Wegener Institute, Helmholtz Centre for Polar and Marine Research (AWI), Bremerhaven, Germany.

Marc Oggier, photograph and biography not available at the time of publication.



**Mats A. Granskog** received the Ph.D. degree in geophysics (hydrosphere) from the University of Helsinki, Helsinki, Finland, in 2004.

He has been with the Oceans and Sea Ice Group, Norwegian Polar Institute, Tromsø, Norway, since 2008, where he is a Senior Research Scientist on sea ice and polar oceanography. His research interests include sea ice geophysics, including sea ice mass and energy balance in the Arctic Ocean.

Allison Fong, photograph and biography not available at the time of publication.



Mario Hoppmann received the Diploma degree in physics from the University of Oldenburg, Oldenburg, Germany, in 2009, and the Ph.D. degree in geosciences from the Jacobs University Bremen, Bremen, Germany, in 2015.

From 2011 to 2015, he was a Ph.D. Student in sea ice physics with the Alfred Wegener Institute, investigating platelet ice and sea ice-ice-shelf-ocean interaction in Antarctica. Since 2015, he has been responsible for the maintenance of a network of autonomous buoys in the central Arctic Ocean. His

research interests include autonomous observations in the polar environment, physical and biological oceanography, sea ice processes, ice-ocean interaction, and the role of the polar regions in the climate system.

Ilkka Matero, photograph and biography not available at the time of publication.

Daniel Scholz, photograph and biography not available at the time of publication.